

See discussions, stats, and author profiles for this publication at: <https://www.researchgate.net/publication/263713058>

Modeling the Interaction of Interferon α -1b to Bovine Serum Albumin as Drug Delivery System.

ARTICLE *in* THE JOURNAL OF PHYSICAL CHEMISTRY B · JULY 2014

Impact Factor: 3.3 · DOI: 10.1021/jp5041713 · Source: PubMed

CITATION

1

READS

13

9 AUTHORS, INCLUDING:



Ying Xie

Peking University

14 PUBLICATIONS 156 CITATIONS

SEE PROFILE

Modeling the Interaction of Interferon α -1b to Bovine Serum Albumin as a Drug Delivery System

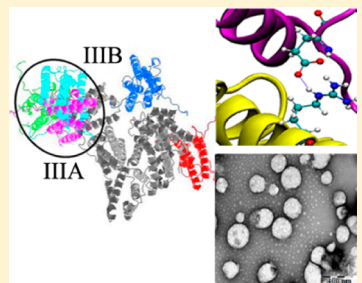
Qi Luo,^{†,§} Yihui Wang,^{‡,§} Hongge Yang,[‡] Chang Liu,[‡] Yuan Ding,[‡] Haifeng Xu,[‡] Qi Wang,[†] Yingchun Liu,^{*,†} and Ying Xie^{*,‡}

[†]Soft Matter Research Center and Department of Chemistry, Zhejiang University, Hangzhou, Zhejiang 310027, P.R. China

[‡]State Key Laboratory of Natural and Biomimetic Drugs, Department of Pharmaceutics, School of Pharmaceutical Sciences, Peking University, Beijing 100191, P.R. China

Supporting Information

ABSTRACT: Protein-based nanoparticles represent a promising approach to carry polypeptide and protein drugs. Using both theory and experimentation, an interferon α -1b (IFN) delivery system carried by bovine serum albumin (BSA) nanoparticles was designed. Theoretical results indicate the most probable binding site and interaction mechanism for IFN on BSA. IFN has a higher binding affinity with BSA compared with small chemical drugs. The drug loading is about 8 mg/g, significantly higher than those reported in other literature. The release profiles differ between the nanoparticles prepared by the incorporation method and the adsorption method. The adsorption of IFN on BSA nanoparticles is monolayer adsorption. The fact that IFN was carried successfully by BSA nanoparticles establishes a solid basis for expanding the drug loading field of BSA nanoparticles to proteins and polypeptides.



INTRODUCTION

Polypeptide and protein drugs have already evolved into mainstream therapeutics and represent a significant portion of the pharmaceutical market.¹ Because of their enzymatic degradation, immunogenic reactions, and poor oral bioavailability, the transport of these polypeptide and protein drugs into the body remains challenging.² Currently, PEGylation strategies,³ liposomes,² microemulsions,⁴ and nanoparticles⁵ provide more opportunities for proteins and polypeptides to overcome these impediments.

Protein-based nanoparticles are particularly promising among the available potential drug carrier systems with apparent advantages such as better stability during storage and *in vivo*, nontoxicity, and nonimmunogenicity.⁶ In addition to the merits mentioned above, albumin shows a special property of preferential uptake in tumor and inflamed tissue, and represents a hopeful strategy for targeted delivery of drugs.⁷ Over the past decades, albumin-based nanoparticles have been proven to be effective and promising carriers for small chemical drugs. Abraxane (paclitaxel-albumin nanoparticles prepared by nabtechnology) has been approved in the United States by the US Food and Drug Administration (FDA) for treatment of breast cancer.⁸ Albumin has also been reported to limit the possibility of protein unfolding, deactivation, or precipitation.² One of the potential applications of albumin is as a carrier for polypeptide and protein drugs. Espuelas et al. demonstrated that bovine serum albumin (BSA) nanoparticles would be a suitable carrier for gamma interferon and can potentiate the therapeutic activity of it.⁹ However, the interaction mechanism between protein drugs and protein carriers remains unknown, especially at the molecular level. Undoubtedly, understanding

the chemical interactions between drugs and carriers is crucial to designing optimized drug delivery systems and improving drug release.¹⁰

Interferons (IFNs) are a group of proteins that nucleated cells secrete in response to infection with a virus, or when appropriately stimulated in other ways.¹¹ As cytokines, IFNs are potent regulators of cell growth and have immunomodulatory activity.¹² In this study, BSA is chosen to carry interferon α -1b (IFN), the first expressing protein cloned from the Chinese interferon gene. This research is supposed to act as an example for studying protein-based drug delivery carrying polypeptide and protein drugs. To deal with the complexity of these interactions, various computational methods are employed to shed light on the details of the interaction mechanism between IFN and BSA, which is clearly difficult when depending on experiments only. Experiments are indispensable for the examination of predictions and practical applications of drug delivery systems. Thus, combination of theory and experimentation is a feasible and effective way to explore drug delivery systems.

To design an IFN delivery system carrying BSA, the most possible binding mode is searched first and the interaction mechanism is illustrated. Then, the free energy of binding of IFN and BSA is calculated. Finally, series of experiments including characterization, adsorption, as well as *in vitro* release are performed according to the predictive results of the interactions between the drug and the carrier.

Received: April 29, 2014

Revised: June 26, 2014

Published: July 2, 2014

METHODS

Refinement of 3D Structures. The initial coordinates of BSA and IFN were selected from the Protein Data Bank, but they were incomplete. For BSA (PDB code 3V03),¹³ two residues were absent at the N-terminal (D1–T2). For IFN (PDB code 3UX9),¹⁴ there were four regions unavailable (S1–S8, G45–K50, E103–M112, N157–E166). To complete their three-dimensional structures, Modeller 9.11¹⁵ was used, which is usually employed to perform homology modeling.

Of the resulting models optimized, one that ranked first was relegated to the molecular dynamics (MD) simulations for refinement using the GROMACS-4.5.2 program package.^{16,17} Each model of BSA and IFN was put in a cubic box, respectively. The AMBER03 all-atom force field¹⁸ was used for describing the proteins solvated with TIP3P water molecules.¹⁹ Both MD simulations were carried out in the isothermal–isobaric (NPT) ensemble with temperature and pressure maintained at 298 K and 101.3 kPa, using the Nosé–Hoover temperature control algorithm²⁰ and the Parrinello–Rahman algorithm,²¹ respectively. The particle-mesh Ewald method²² was used to describe long-range electrostatic interactions with a cutoff of 12 Å for the separation of the direct and reciprocal space summation. Lennard-Jones interactions were truncated between 10 and 11 Å with a smooth switching of the potential. Covalent bonds involving hydrogen atoms were constrained to their equilibrium lengths through the LINCS algorithms.²³ A time step of 2 fs was used, and trajectories were saved every 10 ps for analysis. Each system was simulated for 5 ns until the three-dimensional structures of proteins were stable and reasonable.

Docking. BSA was regarded as the receptor with the ligand IFN. Docking of IFN to BSA was performed with ZDOCK Server (v3.0.2, <http://zdock.umassmed.edu/>).²⁴ The optimized 3D structures of proteins were submitted to the server. According to the scoring function of ZDOCK, the top 5 ZDOCK models were optimized with rigid body docking and the ligand center-of-mass positions for the top 500 ZDOCK models were given. Models representing three different domains were selected. Because the flexibility of proteins was not taken into account by ZDOCK Server, MD simulations were used again to predict the binding site starting from models above.

MD Simulations. 30 ns MD simulations of models representing three different domains were performed using the GROMACS-4.5.2 program package^{16,17} with the same parameters as used in the section Refinement of 3D Structures. Then, the interaction energy and hydrogen bonds between IFN and BSA in each system were calculated according to the trajectory of the last 2 ns. We found one of three models has much stronger interaction and more hydrogen bonds than the other two models; thus, we chose this model called model 2 as a rational candidate to perform the following steered MD simulations.

Steered MD Simulations and Umbrella Sampling. During the 2800 ps steered MD (SMD) simulation, the backbone of BSA was fixed, whereas the flexible side-chain movements were allowed. IFN remained unrestrained. BSA served as a reference, and IFN was pulled away with increasing center-of-mass (COM) distance from the reference along the negative direction of the z-axis, using a spring constant of 1000 kJ/mol and a pull rate of 0.001 nm/ps. Application of faster pulling rates (0.002 and 0.01 nm/ps) resulted in less accurate

force versus time curves (Figure S1, Supporting Information); thus, the slower pulling rate was applied to ensure reliability of the results.

From the SMD trajectory, snapshots were extracted to generate the starting configurations for each umbrella sampling window.²⁵ An asymmetric distribution of sampling windows was used. First, the window spacing was set to 0.2 nm. Then, on this basis, a smaller window spacing (0.1 nm or even 0.05 nm) was used at some points to ensure sufficient overlap between adjacent windows, and resulted in 28 windows. In each window, 12 ns MD was performed for umbrella sampling. Analysis of results was performed with the weighted histogram analysis method (WHAM).²⁶ Statistical errors were estimated with bootstrap analysis.²⁷

Preparation of IFN–BSA Nanoparticles. In the incorporation method, both BSA and IFN could sediment together to form nanoparticles in the process when the solubility of them was reduced by transferring solvent.²⁸ Briefly, BSA and IFN were dissolved in distilled water at a mass ratio of 80:1. Ethanol was continuously dropped into the solution under stirring of 500 rpm until the nanoparticles formed completely. Glutaraldehyde-ethanol solution (0.4%, 40 μL) was added to stabilize the nanoparticles and the stirring continued for 3 h. Suspensions of IFN–BSA nanoparticles were obtained after the ethanol was removed by reduced pressure distillation under 313 K in a water bath.

In the adsorption method, blank BSA nanoparticles were prepared first according to the transferring solvent method described above. IFN would adhere onto the surface of blank BSA nanoparticles to form IFN–BSA nanoparticles at a certain condition. Briefly, BSA was dissolved in distilled water and ethanol was continuously dropwise added. Glutaraldehyde-ethanol solution (0.4%, 40 μL) was added under stirring of 500 rpm. The blank BSA nanoparticle suspensions were prepared after ethanol was removed by reduced pressure distillation under 313 K in a water bath. A certain amount of IFN was incubated with the blank BSA nanoparticles for 30 min (pH 5.5, temperature = 277 K) to promise the adsorption of IFN on the surface of BSA nanoparticles.

Determination of Encapsulation Efficiency/Drug Loading. The ability of BSA loading IFN was expressed by encapsulation efficiency (ee) or drug loading (DL). ee refers to the ratio of IFN encapsulated in the IFN–BSA, and DL refers to the mass of IFN in 1 g of nanoparticles. It was convenient to monitor the content of IFN loaded in the nanoparticles by using a spectrophotometer (Cary Eclipse, USA), since IFN was labeled with FITC.²⁹

IFN was substituted by FITC–IFN in the preparation. Free FITC–IFN was separated from FITC–IFN–BSA nanoparticles by centrifugation at 14 000 rpm for 20 min. The concentration of free FITC–IFN in supernatant was calculated from the standard relationship between the adsorption intensity and the concentration of free FITC–IFN, in which the adsorption intensity was determined at excitation wave 491 nm and emission wave 518 nm. The formulas of ee and DL were respectively as follows:

$$\text{ee (\%)} = \left[1 - \frac{(c_{\text{FITC-IFN}})_{\text{supernatants}} \times V}{(m_{\text{FITC-IFN}})_{\text{total}}} \right] \times 100\% \quad (1)$$

$$\text{DL} = \frac{\text{ee} \times m_{\text{IFN}}}{m_{\text{BSA}} + m_{\text{IFN}}} \quad (2)$$

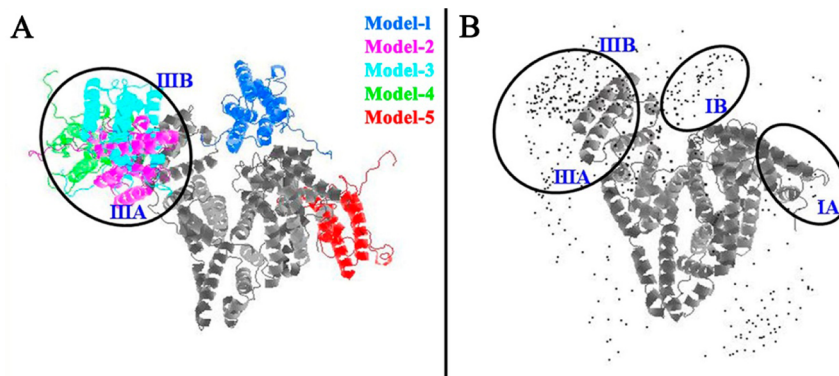


Figure 1. Models optimized by ZDOCK Server. (A) The top 5 models. BSA is shown in gray, while the colored ligand represents IFN in each model. (B) The ligand center-of-mass positions (small black dots) for the top 500 ZDOCK models.

where V represents the volume of the supernatant (mL), $(m_{\text{FITC-IFN}})_{\text{total}}$ the whole quantity of FITC-IFN in the preparation, and $(C_{\text{FITC-IFN}})_{\text{supernatants}}$ the concentration of free FITC-IFN in supernatant. m_{IFN} and m_{BSA} are the dosages of IFN and BSA, respectively.

Characterization of IFN-BSA Nanoparticles. IFN-BSA nanoparticles were diluted by distilled water. After being filtered with a $0.45 \mu\text{m}$ filter membrane, the mean grain size and PDI (polydispersity index) of IFN-BSA nanoparticle suspensions were determined by a Nano Series Zen 4003 Zeta sizer (Malvern Instruments Ltd. UK), with the following parameters: 298 K, running for 15 times, equilibrium time of 60 s. A transmission electron microscope (JEOL 1200EX TEM, JEOL. Ltd. Jpn) was adopted to observe the morphology of IFN-BSA nanoparticles.

Adsorption Behavior of IFN on BSA Nanoparticles. In the adsorption method, the effect of different IFN concentrations on the adsorption behavior was studied. The mass ratio IFN/BSA (W/W) was 1/40, 1/80, and 1/120. When adsorption equilibrium was reached, nanoparticles were separated from the free IFN solution by centrifugation at 14 000 rpm for 20 min. Then, the concentration of IFN in supernatant (c , mg/L) and the ee were measured as described above. The adsorption quantity (q , mg/g), the mass of IFN carried by 1 g of BSA, was calculated with the following formula:

$$q (\text{mg/g}) = \frac{\text{ee} \times m_{\text{IFN}}}{m_{\text{BSA}}} \quad (3)$$

The relationship between q and c was evaluated according to the Freundlich adsorption equation, $\ln q = K + N \ln c$, in which K and N were constants related to the temperature and the characteristics of BSA and IFN. In the experiment, IFN was labeled with FITC to make the measurement easier.

In Vitro Release of IFN from BSA Nanoparticles. IFN-BSA nanoparticles prepared with either the incorporation method or the adsorption method were resuspended with 100 mL of pH 7.2 PBS (phosphate buffered saline, 0.01 mol/L) at 310 ± 0.5 K. Under 100 rpm stirring, a 1 mL sample was taken out at given times of 5, 10, 30, 60, 120, and 240 min and 1 mL of fresh medium was supplied meanwhile. The released IFN concentration (c_{sample} , $\mu\text{g/mL}$) in supernatant was determined with a spectrofluorometer after centrifugation at 14 000 rpm for 20 min. The release of IFN from IFN-BSA in serum was proceeded as described above in which 10% FCS (fetal calf serum) dissolved into PBS as release medium. The cumulative

release proportion (CRP) at a given time was calculated with the following formula:

$$\text{CRP (\%)} = \frac{c_{\text{sample}} \times 100 + \sum (c_{\text{previously samples}} \times 1)}{m_{\text{total}}} \times 100\% \quad (4)$$

in which $c_{\text{previously samples}}$ is the concentration of IFN in supernatant at a previously given time, m_{total} is the total mass of IFN in IFN-BSA nanoparticles, 100 represents the volume of release medium, and 1 represents the sample volume at each given time. In the experiment, IFN was labeled with FITC to make the measurement easier.

RESULTS AND DISCUSSION

Binding Mode. The top 5 models optimized by ZDOCK Server are models 1, 2, 3, 4, and 5. Figure 1A shows the position of IFN around BSA in each model. The tertiary structure of BSA is formed by three homologous domains I \rightarrow III, each of which is divided into two subdomains A and B.^{30,31} Models 1 and 5 are in subdomain IB and subdomain IA, respectively. Models 2, 3, and 4 are all located in domain III, crossing both subdomains IIIA and IIIB. In addition, the ligand center-of-mass positions for the top 500 ZDOCK models are shown in Figure 1B. The probability of mass positions of the ligand center in domain III is much greater than that in subdomains IA and IB. Moreover, subdomain IIIA is one of the most widely reported drug binding sites.^{32,33} Therefore, domain III of BSA may be the most probable binding site for IFN. Furthermore, the highest ranking model in domain III, model 2, is the most probable binding mode in the present work.

MD simulations were performed to relax the resulting structures after ZDOCK as a complement to rigid body docking. Therefore, the binding mode between IFN and BSA has become more stable and reasonable in each model. Table 1 shows that the interaction energy between IFN and BSA in model 2 is more negative than that in models 1 and 5, which suggests that IFN shows a greater affinity to BSA in model 2 than that in models 1 and 5. Moreover, model 2 has a larger number of hydrogen bonds between IFN and BSA than models 1 and 5. Thus, model 2 is proven to be the most probable binding mode, which is in agreement with the prediction described above. Although model 1 ranks first according to the scoring function of ZDOCK, model 2 proves to be more reasonable than model 1, which indicates MD is an effective method to overcome the limitation of docking. The

Table 1. Interaction Energy (kJ/mol) and the Number of Hydrogen Bonds between IFN and BSA^a

	E_{int}^b	E_{ele}	E_{vdw}	no. of H-bonds ^c
model 1	-397 ± 52	-287 ± 55	-110 ± 12	4 ± 1
model 2	-932 ± 36	-651 ± 41	-281 ± 17	9 ± 1
model 5	-623 ± 102	-414 ± 94	-209 ± 28	6 ± 2

^aIn all the tables in this paper, a number that follows the ± sign is a standard deviation (SD). ^b $E_{\text{int}} = E_{\text{ele}} + E_{\text{vdw}}$, where E_{int} is the interaction energy, E_{ele} the electrostatic interaction, and E_{vdw} the van der Waals interaction. ^cThe average number of hydrogen bonds per time frame.

combination of the two methods can achieve more accurate results than either alone.

Critical Interaction Points. The force and the COM distance along the z-axis during SMD simulation are shown in Figure 2A. From 0 to 755 ps, the force increases dramatically while the COM distance has a change of 0.1 nm. Since 755 ps, however, the COM distance begins to rise obviously, indicating IFN is being pulled apart. Note that the force almost stays around 680 kJ/mol/nm until it begins to decline from 891 ps. Thus, it suggests that certain important interactions between IFN and BSA, which require a large pulling force, have broken during this period. Another noteworthy point is at 1445 ps, where the force falls sharply with a remarkable rise in the COM distance, which means the interaction declines between the two proteins. Some key points, where hydrogen bonds or salt bridges break, are marked with red arrows on the force profile. Their disappearance may explain some changes of the force and the COM distance.

Figure 2B shows the number of hydrogen bonds versus time during SMD simulation. Following a similar trend of force, the number of hydrogen bonds sees a fall as IFN is pulled away since 755 ps. Corresponding to the sharp change of the force and the COM distance, certain hydrogen bonds suddenly break at 1445 ps, which is an important interaction key point. After that, the number fluctuates within a narrow range from 0 to 2 until complete disappearance. The number of hydrogen bonds changes in a similar manner with the force, suggesting that hydrogen bonds play a significant part in the binding of the two proteins. In Figure 2C, the snapshots at some key points illustrate the relative positions for two proteins during SMD, indicating that the secondary structures of the proteins have been maintained. Therefore, we consider that the method used in this work is reasonable.

Interaction Mechanism. Interfacial hydrogen bonds and salt bridges were analyzed in more detail to understand the interaction mechanism at the atomic level. Considering the duration and geometries, two main hydrogen bonds (HB_1 and HB_2) and three main pairs of salt bridges (S_1 – S_3) across protein–protein interfaces are shown in Table 2. In terms of the measurements of the hydrogen bond strength, the geometries illustrate that the two hydrogen bonds always maintain normal strength (the hydrogen–acceptor distance is about 2 Å, and the bond angle is about 160°^{34,35}), although IFN is pulled constantly away from BSA. In other words, breaking these two hydrogen bonds is not easy. Aside from the hydrogen bond HB_1 , a salt bridge S_1 also forms between the guanidinium group of Arg125 and the carboxylate group of Glu503. Thus, the interaction between Arg125 and Glu503 is one of the significant interactions between the two proteins.

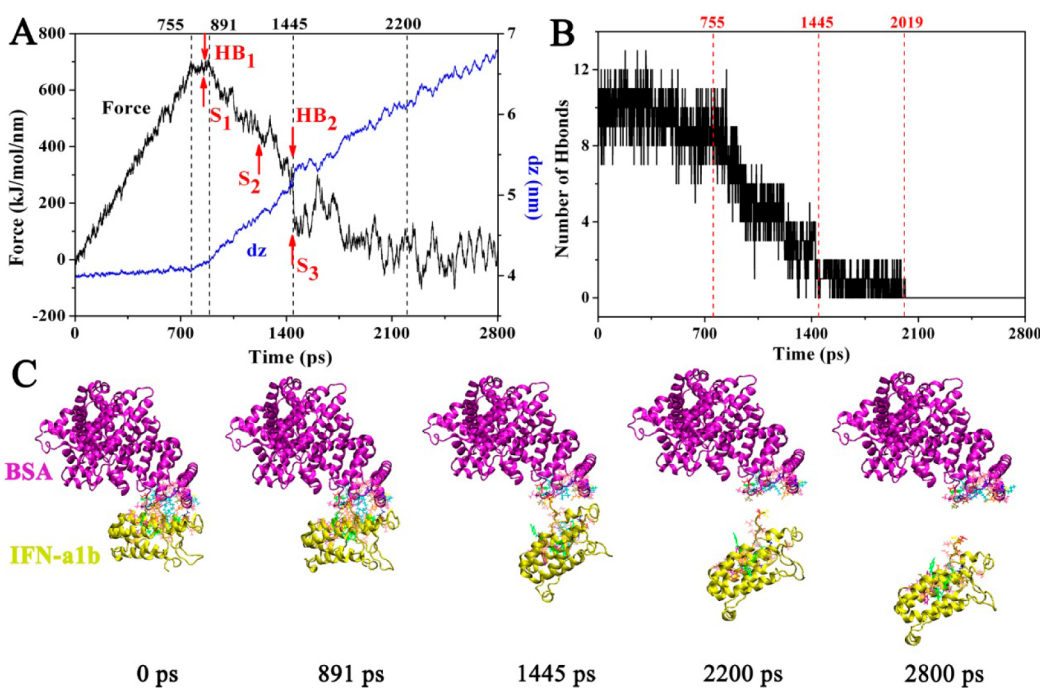


Figure 2. (A) The force and the COM distance along the z-axis (represented by dz) versus time during SMD simulation. Some key points, where the most critical hydrogen bonds or salt bridges break, are marked with red arrows. Hydrogen bonds are HB_1 (Arg125:HE–Glu503:OE2) and HB_2 (Asp2:H–Asp493:O). Salt bridges are S_1 (Arg125:NH2–Glu503:OE1), S_2 (Glu5:OE1–Lys537:NZ), and S_3 (Glu97:OE2–Lys537:NZ). In this paper, the first residue is from IFN and the second residue is from BSA in all of the pairs. (B) The number of hydrogen bonds versus time during SMD simulation. Some key points are marked by a red dash. (C) Snapshots at the key points along the dissociation pathway. The residues in a binding site are shown in a line model.

Table 2. Duration and Geometries of Hydrogen Bonds (HB_1 and HB_2) and Salt Bridges (S_1 – S_3) across Protein–Protein Interfaces^a

code	residue pairs	duration ^b (ps)	dist ^c (Å)	$\langle \text{angle} \rangle^d$
HB_1	Arg125:HE–Glu503:OE2	0–860	2.0 ± 0.4	160.0 ± 11.8
HB_2	Asp2:H–Asp493:O	0–1445	2.0 ± 0.3	160.1 ± 12.2
S_1	Arg125:NH2–Glu503:OE1	0–851	2.9 ± 0.3	
S_2	Glu5:OE1–Lys537:NZ	0–1219	2.9 ± 0.2	
S_3	Glu97:OE2–Lys537:NZ	0–1440	3.1 ± 0.4	

^aThe first residue is from IFN and the second residue is from BSA in all the residue pairs. ^bThe hydrogen bonds or the salt bridges break at the end of duration. ^cDist means the hydrogen–acceptor distance in hydrogen bonds or the donor–acceptor distance in salt bridges in the duration. ^d $\langle \text{angle} \rangle$ means the donor–hydrogen–acceptor angle in the duration.

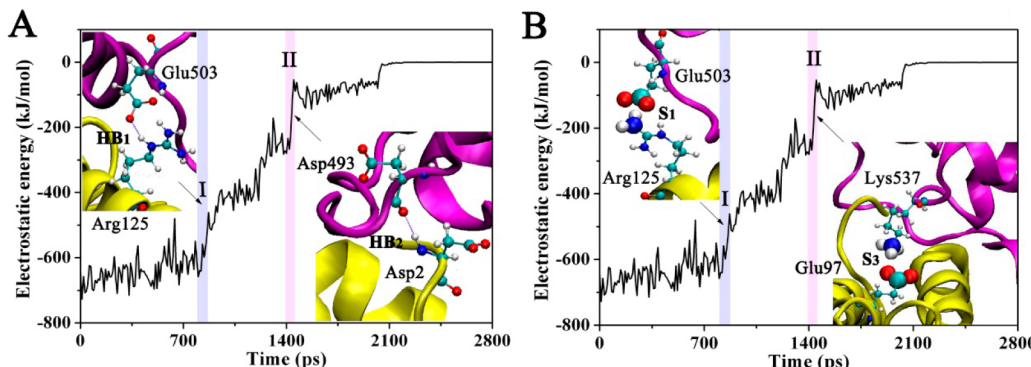


Figure 3. Change of the electrostatic energy between IFN and BSA as a function of time caused by hydrogen bonds and salt bridges. BSA is colored in purple, and IFN is colored in yellow. Areas I and II are the areas where the electrostatic energy sharply decreased (colored in violet and pink, respectively). (A) Hydrogen bonds HB_1 and HB_2 . The black dashed line means the hydrogen bonds HB_1 and HB_2 between hydrogen and acceptor. (B) Salt bridges S_1 and S_3 . The charged groups of salt bridges are shown in the VDW model. All the pairs are shown in the CPK model.

Electrostatic interaction is the main component of the total interaction energy between the two proteins, as shown in Table 1. Figure 3 illustrates that the electrostatic interaction between IFN and BSA decreases markedly when these key hydrogen bonds (Figure 3A) and salt bridges (Figure 3B) break. Because of the existence of a hydrogen bond as well as a salt bridge, the detachment of Arg125 and Glu503 makes a significant contribution to the change of electrostatic energy (area I). In area II, the sharp change may be ascribed to the disappearance of the hydrogen bond Asp2:H–Asp493:O and the salt bridge Glu97:OE2–Lys537:NZ, which break practically at the same time. Since these critical hydrogen bonds and salt bridges are closely related to the change of both pulling force and electrostatic energy, we can deduce that these pairs are crucial for the binding of IFN and BSA. As reported by Nussinov et al., interfacial hydrogen bonds and salt bridges are the major contributors to the electrostatic interactions, which play an important role across protein–protein interfaces.³⁵

Compared with hydrogen bonds and salt bridges, water bridges with an intervening water molecule are serving a supporting role in the interaction between the two proteins. Unlike the hydrogen bonds, the number of water bridges has no evident downward trend, as shown in the inset of Figure 4. This phenomenon is attributed to the fact that the interactions between interface water molecules and proteins are weaker than the hydrogen bonds between the two proteins. Water molecules may insert between two residues and form water bridges at any moment, thus preventing IFN from being pulled away from BSA. However, disrupting the water bridges by force is also easy. Consequently, the intermittent formation and breaking of water bridges leads to the fluctuations in the number markedly.

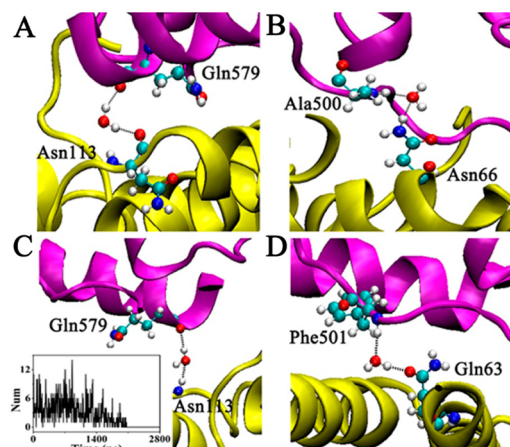


Figure 4. Four types of water bridges between IFN and BSA. BSA is colored in purple, and IFN is colored in yellow. (A) Donor–donor (DD). (B) Acceptor–acceptor (AA). (C) Donor–acceptor (DA). IFN acts as a donor and BSA as an acceptor. (D) Acceptor–donor (AD). IFN acts as an acceptor and BSA as a donor. The inset shows the number of water bridges (Num) versus time during SMD simulation.

Since water molecules can simultaneously donate and accept two hydrogen bonds, four possible types of water bridges must be considered, namely, donor–donor (DD), acceptor–acceptor (AA), donor–acceptor (DA), and acceptor–donor (AD),³⁶ as illustrated by the four representative water bridges in Figure 4. These four pairs were selected because they are the most stable in each type. All of the major water bridges are listed in Table 3. Comparing the four types, DD has the dominant position because of the two stable and long-time water bridges (Asn113–Gln579, Asn66–Val497), in which the intervening

Table 3. Water Bridges across Protein–Protein Interfaces^a

type	water bridge ^b	duration (ps)	times of replacement ^c
DD	<u>Asn113–Gln579</u>	0–1315	2
	Asn66–Val497	0–870	2
	Asp2–Glu494	1425–1615	7
	Asp2–Pro492	20–1410	11
AA	<u>Asn66–Ala500</u>	0–720	5
DA	<u>Asn113–Gln579</u>	550–1325	2
	Lys121–His534	340–895	3
	Cys1–Tyr496	1550–2030	4
AD	<u>Gln63–Phe501</u>	265–775	2
	Ala114–Gln579	1080–1270	6
	Glu97–Lys537	5–1390	12

^aThe first residue is from IFN and the second residue is from BSA in all the residue pairs. ^bThe water bridge with the strongest stability in each type is underlined. ^cAs water molecules are movable, it is possible for the intervening water molecule to be replaced by another. The less times of replacement, the more stable the water bridge.

water molecules are replaced only twice. AA plays a minor role because the sole water bridge is unstable. Interestingly, two stable water bridges are formed between Asn113 and Gln579, as shown in Figure 4A and C. Therefore, the interaction between Asn113 and Gln579 is evidently conducive to the binding of IFN and BSA. Another noticeable pair is Cys1–Tyr496, because the water bridge probably accounts for the attachment of the N-terminal of IFN to BSA from about 1500 to 2000 ps before the two proteins completely separate.

Free Energy. Umbrella sampling simulations were used to determine the free energy (ΔG) of the binding of IFN and BSA. The potential of mean force (PMF) curve was reasonable along the reaction coordinate (as shown in Figures S2 and S3, Supporting Information). Figure 5 shows that the ΔG for the

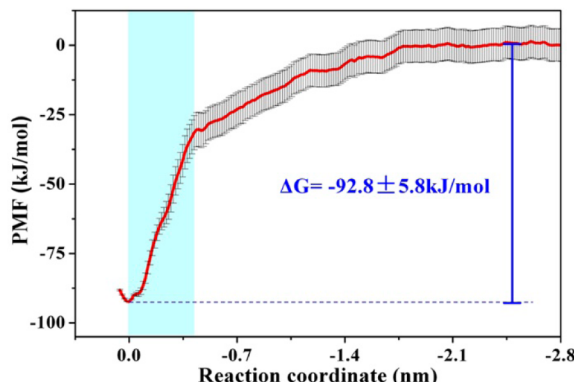


Figure 5. Potential of mean force (PMF) curve for the binding of IFN and BSA. The error bars are shown in black lines. The reaction coordinate is shifted from the z -axis. There is a sharp increase in the area colored in blue, which happens during a period from 780 to 985 ps with some critical interactions destroyed.

binding process is -92.8 ± 5.8 kJ/mol, and this negative value indicates that it is feasible to prepare BSA nanoparticles loading IFN, which is also confirmed by the experimental results.

Compared with some small molecule drugs, IFN shows a higher binding affinity with BSA. For small chemical drugs, ΔG can be calculated from the binding constant (K_B) according to the equation $\Delta G = -RT \ln K_B$. The values of ΔG of binding for small molecule drugs and BSA range from -29.2 to -21 kJ/mol^{37–39} (detailed data in Table S1, Supporting Information),

much more positive than that between IFN and BSA (-92.8 ± 5.8 kJ/mol).

PMF increases substantially within a small range of reaction coordinates. This finding illustrates some critical interactions contribute to the majority of ΔG , that must have been destroyed during this period. The pair Arg125–Glu503 is considered to play an important role in leading to the sharp change in PMF, because both the strong hydrogen bond and salt bridge formed between them have been broken during this period. As Bogen et al. reported, arginine, tryptophan, and tyrosine are much more likely to be hot spots, which have more energetic contributions to protein binding than other amino acids.⁴⁰ Thus, Arg125 in IFN may be a hot spot for the binding of IFN and BSA.

Characterization of IFN–BSA Nanoparticles. The characterization of IFN–BSA nanoparticles prepared using the incorporation method is similar to that of the adsorption method (shown in Table 4, and the size distribution is shown in

Table 4. ee, DL, Size, and PDI of Nanoparticles

characteristics	incorporation method	adsorption method
ee (%)	71.38 ± 3.91	64.99 ± 0.90
DL (mg/g)	8.81 ± 0.48	8.02 ± 0.11
size (nm)	235.0 ± 5.7	254.3 ± 9.8
PDI	0.135	0.162

Figure S4, Supporting Information). The ee is more than 65%, which confirms the feasibility of BSA nanoparticles carrying IFN in the experiments. The DL of IFN in BSA is about 8 mg/g, which is 8 times higher than the reported 1 mg/g.⁹ This result means that one IFN molecule is carried by 30 BSA molecules on average. However, not all the BSA molecules interact with IFN molecules because of the limitation in space. The fact that IFN is carried by BSA efficiently indicates the interaction mechanism explained from the view of calculations. From the docking and MD results, three potential binding sites of BSA (IA, IB, and III) have been found. Domain III proves to be the most important binding site, which can account for the effective binding between IFN and BSA mainly by hydrogen bonds (Arg125–Glu503, Asp2–Asp493) and salt bridges (Arg125–Glu503, Glu5–Lys537, Glu97–Lys537).

TEM micrographs (Figure 6) show that IFN–BSA nanoparticles are spherical, round, and uniform in particle size. Thus,

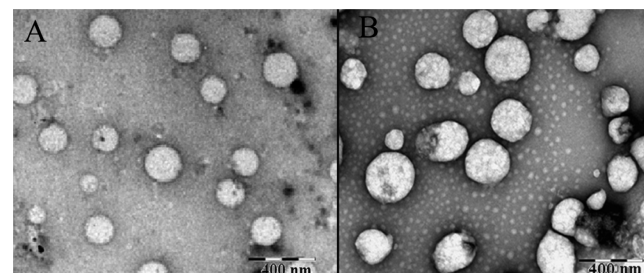


Figure 6. TEM micrographs of IFN–BSA nanoparticles. (A) Incorporation method. (B) Adsorption method.

IFN–BSA nanoparticles obtained from the two methods have no significant difference in morphology. The particle size from TEM, which is about 250 nm, coincides with the result from dynamic laser scattering, which is about 235–254 nm (Figure S4, Supporting Information).

Monolayer Adsorption of IFN on BSA Nanoparticles. During the search for the interactions of IFN with BSA in the adsorption method, it was noticed that the adsorption process of IFN onto BSA agreed with the Freundlich adsorption equation. As shown in Table S, the adsorptive quantity (q , mg/

Table 5. Adsorptive Quantity and ee for Different BSA/IFN (W/W)

BSA/IFN (W/W)	equilibrium concentration of IFN (c , mg/L)	adsorptive quantity (q , mg/g)	ee (%)
120:1	8.41 ± 0.30	5.67 ± 0.09	68.04 ± 1.15
80:1	13.47 ± 0.34	8.12 ± 0.11	64.99 ± 0.90
40:1	33.27 ± 0.39	13.36 ± 0.13	53.43 ± 0.54

g) and ee for different IFN concentrations (c , mg/L) were measured under the same conditions (pH 5.5, temperature = 277 K, incubation time = 1 h). Using the Freundlich adsorption equation, the origin of the coordinates and the data in Table S were used for linear fitting (shown in Figure S5, Supporting Information), which suggests that IFN absorbs on BSA nanoparticles with the mechanism of monolayer adsorption. The binding sites of BSA are occupied by the first layer of IFN, and it is difficult for IFN to form the second layer on the surface of BSA nanoparticles.

In Vitro Release of IFN from BSA Nanoparticles. The *in vitro* release profile of IFN from BSA nanoparticles in PBS could reflect the combination ability and manner between IFN and BSA, and it is helpful in revealing the interaction behavior. According to the results shown in Figure 7, the release rate of

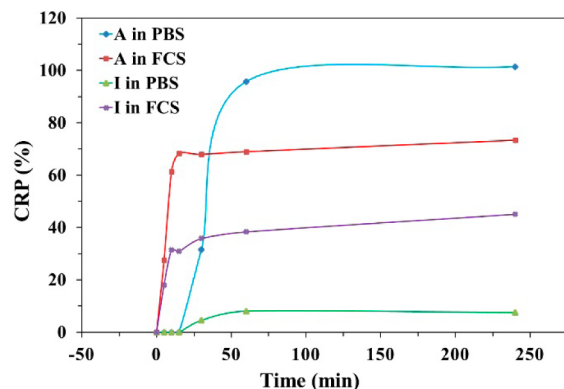


Figure 7. *In vitro* release profile of IFN-BSA nanoparticles prepared with the adsorption method (abbreviated as A) or incorporation method (abbreviated as I). PBS (0.01 mol/L) and 10% FCS are the release mediums.

IFN-BSA nanoparticles prepared with the incorporation method is extremely slow that the cumulative release proportion does not exceed 20% at 4 h, while IFN could be released quickly from BSA nanoparticles at 100% at 1 h when it is prepared with the adsorption method. The different release profile of IFN-BSA nanoparticles between the two preparation methods may result from the different sites of IFN molecules in BSA nanoparticles. In the incorporation method, IFN is embedded into nanoparticles because IFN combines initially with BSA and then deposits together to form nanoparticles. In the adsorption method, IFN adheres on the surface of BSA nanoparticles, as blank BSA nanoparticles are prepared first, followed by the addition of IFN at low temperature. Although

the preparation methods are different, the DL and ee of IFN-BSA nanoparticles are the same. It shows that a coincidental quantity relationship exists between IFN and BSA and the coupling efficiency is independent of preparation methods.

The release of IFN-BSA prepared with both the adsorption method and the incorporation method in FCS is faster than that in PBS (shown in Figure 7). This is caused by the combination of IFN with serum protein and fibrinogen in FCS. The total CRP% of IFN from IFN-BSA is lower than 80% in FCS, which confirms that part of the released IFN combines with serum protein and has been centrifuged during the test. Thus, it is necessary to adopt some strategies such as PEG modification⁴¹ to avoid IFN being cleared from blood when it is in clinical applications.

CONCLUSIONS

In order to design a new protein-based drug delivery system, calculations were performed to guide the experiments, which in turn verified the theoretical results. The calculation predicted that domain III of BSA is the most potential binding site for IFN, accounting for the effective binding between them. Hydrogen bonds and salt bridges play a significant role in the binding as two forms of electrostatic interaction. The four types of water bridges also serve a supporting role in the interaction. The free energy of the binding process indicates IFN has a higher binding affinity with BSA than small chemical drugs. Both the incorporation method and the adsorption method can be utilized to prepare IFN-BSA nanoparticles. The encapsulation efficiency and the drug loading of IFN in BSA are significantly higher than those reported in other literature. However, the release rate of IFN from BSA nanoparticles in the adsorption method is much faster than that in the incorporation method in both PBS and FCS. As the binding site, domain III of BSA is occupied by IFN, and the adsorption of IFN on BSA is a monolayer adsorption, in accordance with the Freundlich adsorption equation.

The understanding of the delivery system carried by BSA may serve as the first step for digging into protein-based drug delivery for polypeptide and protein drugs, and may be useful in designing more efficient drug delivery and release systems in the future.

ASSOCIATED CONTENT

S Supporting Information

Force versus time plots using different pulling rates (Figure S1). The convergence of potential of mean force (PMF) curves of every 2 ns (Figure S2). The umbrella histogram (Figure S3). The size distribution by intensity of IFN-BSA nanoparticles (Figure S4). The relationship between adsorptive capacity (q , mg/g) and equilibrium concentration of IFN (c , mg/L) (Figure S5). The binding constant (K_B) and free energy of binding for small molecule drugs and BSA (Table S1). This material is available free of charge via the Internet at <http://pubs.acs.org>.

AUTHOR INFORMATION

Corresponding Authors

*Phone: +86 571 87952424. Fax: +86 571 87951895. E-mail: liuyingch@zju.edu.cn.

*Phone: +86 10 82801508. Fax: +86 10 82801575. E-mail: bmuxieying@bjmu.edu.cn.

Author Contributions

[§]Q.L. and Y.W. contributed equally to this work.

Notes

The authors declare no competing financial interest.

ACKNOWLEDGMENTS

This work was financially supported by the National Natural Science Foundation of China (Nos. 21273200, J1210042, and 81202469) and Founder of new drug research fund (No. 201311).

REFERENCES

- (1) Katsila, T.; Siskos, A. P.; Tamvakopoulos, C. Peptide and Protein Drugs: The Study of their Metabolism and Catabolism by Mass Spectrometry. *Mass Spectrom. Rev.* **2012**, *31*, 110–133.
- (2) Solaro, R.; Chiellini, F.; Battisti, A. Targeted Delivery of Protein Drugs by Nanocarriers. *Materials* **2010**, *3*, 1928–1980.
- (3) Milla, P.; Dosio, F.; Cattel, L. Pegylation of Proteins and Liposomes: A Powerful and Flexible Strategy to Improve the Drug Delivery. *Curr. Drug Metab.* **2012**, *13*, 105–119.
- (4) Liu, D. Y.; Kobayashi, T.; Russo, S.; Li, F. L.; Plevy, S. E.; Gambling, T. M.; Carson, J. L.; Mumper, R. J. In Vitro and in Vivo Evaluation of a Water-in-Oil Microemulsion System for Enhanced Peptide Intestinal Delivery. *AAPS J.* **2013**, *15*, 288–298.
- (5) Lee, H. J.; Park, H. H.; Kim, J. A.; Park, J. H.; Ryu, J.; Choi, J.; Lee, J.; Rhee, W. J.; Park, T. H. Enzyme Delivery Using the 30Kc19 Protein and Human Serum Albumin Nanoparticles. *Biomaterials* **2014**, *35*, 1696–1704.
- (6) Elzoghby, A. O.; Samy, W. M.; Elgindy, N. A. Protein-Based Nanocarriers as Promising Drug and Gene Delivery Systems. *J. Controlled Release* **2012**, *161*, 38–49.
- (7) Elzoghby, A. O.; Samy, W. M.; Elgindy, N. A. Albumin-Based Nanoparticles as Potential Controlled Release Drug Delivery Systems. *J. Controlled Release* **2012**, *157*, 168–182.
- (8) Vishnu, P.; Roy, V. Safety and Efficacy of Nab-Paclitaxel in the Treatment of Patients with Breast Cancer. *Breast Cancer: Basic Clin. Res.* **2011**, *5*, 53–65.
- (9) Segura, S.; Gamazo, C.; Irache, J. M.; Espuelas, S. Gamma Interferon Loaded Onto Albumin Nanoparticles: In Vitro and in Vivo Activities Against Brucella Abortus. *Antimicrob. Agents Chemother.* **2007**, *51*, 1310–1314.
- (10) Albers, J.; Alles, R.; Matthee, K.; Knop, K.; Nahrup, J. S.; Kleinebudde, P. Mechanism of Drug Release From Polymethacrylate-Based Extrudates and Milled Strands Prepared by Hot-Melt Extrusion. *Eur. J. Pharm. Biopharm.* **2009**, *71*, 387–394.
- (11) Foster, G. R.; Finter, N. B. Are All Type I Human Interferons Equivalent? *J. Viral Hepatitis* **1998**, *5*, 143–152.
- (12) Katze, M. G.; He, Y. P.; Gale, M. Viruses and Interferon: A Fight for Supremacy. *Nat. Rev. Immunol.* **2002**, *2*, 675–687.
- (13) Majorek, K. A.; Porebski, P. J.; Dayal, A.; Zimmerman, M. D.; Jablonska, K.; Stewart, A. J.; Chruszcz, M.; Minor, W. Structural and Immunologic Characterization of Bovine, Horse, and Rabbit Serum Albumins. *Mol. Immunol.* **2012**, *52*, 174–182.
- (14) Ouyang, S. Y.; Gong, B.; Li, J. Z.; Zhao, L. X.; Wu, W.; Zhang, F. S.; Sun, L. N.; Wang, S. J.; Pan, M.; Li, C.; et al. Structural Insights Into a Human Anti-Influenza Antibody Exerting Therapeutic Potential for Systemic Lupus Erythematosus. *J. Mol. Med.* **2012**, *90*, 837–846.
- (15) Eswar, N.; Webb, B.; Marti-Renom, M. A.; Madhusudhan, M. S.; Eramian, D.; Shen, M.; Pieper, U.; Sali, A. Comparative Protein Structure Modeling Using Modeller. *Curr. Protoc. Bioinf.* **2006**, *15*, 5–6.
- (16) Van der Spoel, D.; Lindahl, E.; Hess, B.; Groenhof, G.; Mark, A. E.; Berendsen, H. Gromacs: Fast, Flexible, and Free. *J. Comput. Chem.* **2005**, *26*, 1701–1718.
- (17) Hess, B.; Kutzner, C.; van der Spoel, D.; Lindahl, E. Gromacs 4: Algorithms for Highly Efficient, Load-Balanced, and Scalable Molecular Simulation. *J. Chem. Theory Comput.* **2008**, *4*, 435–447.
- (18) Duan, Y.; Wu, C.; Chowdhury, S.; Lee, M. C.; Xiong, G. M.; Zhang, W.; Yang, R.; Cieplak, P.; Luo, R.; Lee, T.; et al. A Point-Charge Force Field for Molecular Mechanics Simulations of Proteins Based On Condensed-Phase Quantum Mechanical Calculations. *J. Comput. Chem.* **2003**, *24*, 1999–2012.
- (19) Jorgensen, W. L.; Chandrasekhar, J.; Madura, J. D.; Impey, R. W.; Klein, M. L. Comparison of Simple Potential Functions for Simulating Liquid Water. *J. Chem. Phys.* **1983**, *79*, 926–935.
- (20) Nose, S. A Unified Formulation of the Constant Temperature Molecular Dynamics Methods. *J. Chem. Phys.* **1984**, *81*, 511–519.
- (21) Parrinello, M.; Rahman, A. Polymorphic Transitions in Single Crystals: A New Molecular Dynamics Method. *J. Appl. Phys.* **1981**, *S2*, 7182–7190.
- (22) Darden, T.; York, D.; Pedersen, L. Particle Mesh Ewald: An $N \log(N)$ Method for Ewald Sums in Large Systems. *J. Chem. Phys.* **1993**, *98*, 10089–10092.
- (23) Hess, B.; Bekker, H.; Berendsen, H.; Fraaije, J. Lincs: A Linear Constraint Solver for Molecular Simulations. *J. Comput. Chem.* **1997**, *18*, 1463–1472.
- (24) Pierce, B. G.; Hourai, Y.; Weng, Z. P. Accelerating Protein Docking in ZDOCK Using an Advanced 3D Convolution Library. *PLoS One* **2011**, *6*, 1–6.
- (25) Lemkul, J. A.; Bevan, D. R. Assessing the Stability of Alzheimer's Amyloid Protofibrils Using Molecular Dynamics. *J. Phys. Chem. B* **2010**, *114*, 1652–1660.
- (26) Kumar, S.; Bouzida, D.; Swendsen, R. H.; Kollman, P. A.; Rosenberg, J. M. The Weighted Histogram Analysis Method for Free-Energy Calculations On Biomolecules. I. The Method. *J. Comput. Chem.* **1992**, *13*, 1011–1021.
- (27) Hub, J. S.; de Groot, B. L.; van der Spoel, D. G. Wham-a Free Weighted Histogram Analysis Implementation Including Robust Error and Autocorrelation Estimates. *J. Chem. Theory Comput.* **2010**, *6*, 3713–3720.
- (28) Weber, C.; Coester, C.; Kreuter, J.; Langer, K. Desolvation Process and Surface Characterisation of Protein Nanoparticles. *Int. J. Pharm.* **2000**, *194*, 91–102.
- (29) Shibata, A.; Abe, H.; Furukawa, K.; Tsuneda, S.; Ito, Y. Protein Detection Using Oligonucleotide Probes. *Nucleic Acids Symp. Ser.* **2009**, *53*, 157–158.
- (30) He, X. M.; Carter, D. C. Atomic Structure and Chemistry of Human Serum Albumin. *Nature* **1992**, *358*, 209–215.
- (31) Jana, S.; Dalapati, S.; Ghosh, S.; Guchhait, N. Binding Interaction Between Plasma Protein Bovine Serum Albumin and Flexible Charge Transfer Fluorophore: A Spectroscopic Study in Combination with Molecular Docking and Molecular Dynamics Simulation. *J. Photochem. Photobiol., A* **2012**, *231*, 19–27.
- (32) Carter, D. C.; He, X. M. Structure of Human Serum Albumin. *Science* **1990**, *249*, 302–303.
- (33) Jana, S.; Ghosh, S.; Dalapati, S.; Guchhait, N. Exploring Structural Change of Protein Bovine Serum Albumin by External Perturbation Using Extrinsic Fluorescence Probe: Spectroscopic Measurement, Molecular Docking and Molecular Dynamics Simulation. *Photochem. Photobiol. Sci.* **2012**, *11*, 323–332.
- (34) Jeffrey, P. D. G. A.; Saenger, P. D. W. *Hydrogen Bonding in Biological Structures*; Springer: Berlin, Heidelberg, 1991.
- (35) Xu, D.; Tsai, C. J.; Nussinov, R. Hydrogen Bonds and Salt Bridges Across Protein-Protein Interfaces. *Protein Eng.* **1997**, *10*, 999–1012.
- (36) Petukhov, M.; Cregut, D.; Soares, C. M.; Serrano, L. Local Water Bridges and Protein Conformational Stability. *Protein Sci.* **1999**, *8*, 1982–1989.
- (37) Agudelo, D.; Bourassa, P.; Bruneau, J.; Berube, G.; Asselin, E.; Tajmir-Riahi, H. A. Probing the Binding Sites of Antibiotic Drugs Doxorubicin and N-(Trifluoroacetyl) Doxorubicin with Human and Bovine Serum Albumins. *PLoS One* **2012**, *7*, 1–13.
- (38) Vishkaee, T. S.; Mohajerani, N.; Nafisi, S. A Comparative Study of the Interaction of Tamiflu and Oseltamivir Carboxylate with Bovine Serum Albumin. *J. Photochem. Photobiol., B* **2013**, *119*, 65–70.
- (39) Solomonov, A. V.; Rumyantsev, E. V.; Antina, E. V. Serum Albumin and its Bilirubin Complex as Drug-Carrier Proteins for Water-Soluble Porphyrin: A Spectroscopic Study. *Monatsh. Chem.* **2013**, *144*, 1743–1749.

- (40) Bogan, A. A.; Thorn, K. S. Anatomy of Hot Spots in Protein Interfaces. *J. Mol. Biol.* **1998**, *280*, 1–9.
- (41) Clark, R.; Olson, K.; Fuh, G.; Marian, M.; Mortensen, D.; Teshima, F.; Chang, S.; Chu, H.; Mukku, V.; CanovaDavis, E.; et al. Long-Acting Growth Hormones Produced by Conjugation with Polyethylene Glycol. *J. Biol. Chem.* **1996**, *271*, 21969–21977.